ChemPubSoc Europe

DOI: 10.1002/chem.201801355

CHEMISTRY A European Journal Full Paper

Macrocyclic Chemistry

# A Unique $Ln^{III}${[3.3.1]$Ga^{III}$ Metallacryptate} Series That Possesses Properties of Slow Magnetic Relaxation and Visible/Near-Infrared Luminescence

Jacob C. Lutter,[a] Svetlana V. Eliseeva,*[b] Jeff W. Kampf,[a] Stéphane Petoud,*[b] and Vincent L. Pecoraro*[a]

**Abstract:** A new family of [3.3.1] metallacryptates with the general composition [$LnGa_6(H_2shi)(Hshi)(shi)_7(C_5H_5N)$] (**Ln-1**; $shi^{3-}$ = salicylhydroximate; Ln = Pr, Nd, Sm–Yb) has been synthesized and characterized. **Ln-1** display both interesting magnetic and luminescent properties. **Sm-1** has sharp emission bands in the visible and the near-infrared (NIR) regions with quantum yield values ($Q^L_{Sm}$) of 1.64(9) and 5.5(2)·$10^{-2}$%, respectively. **Tb-1** exhibits a weak green emission ($Q^L_{Tb}$ = 1.89(3)·$10^{-1}$%) while **Pr-1**, **Nd-1**, **Ho-1**, **Er-1**, and **Yb-1** possess emission bands in the NIR range with $Q^L_{Pr}$ = 3.7(2)·$10^{-3}$%, $Q^L_{Nd}$ = 1.71(5)·$10^{-1}$%, $Q^L_{Ho}$ = 1.1(2)·$10^{-3}$%, $Q^L_{Er}$ = 7.1(2)·$10^{-3}$% and $Q^L_{Yb}$ = 0.65(3)%. **Nd-1**, **Dy-1**, and **Yb-1** display slow magnetization relaxation in an applied field, where only **Dy-1** has been observed to follow an Orbach process ($U_{eff}$ = 12.7 K). The combination of NIR emission with magnetic properties makes **Nd-1** and **Yb-1** attractive candidates as smart materials addressable in two manners.

## Introduction

Over the past few decades, significant research interest has been focused on lanthanide(III) metal ions ($Ln^{3+}$) and compounds formed with them. The inherent nature of the valence 4f electrons leads to very interesting properties, especially in terms of luminescence and magnetism. The 4f electrons are shielded by the 5s and 5p orbitals, inhibiting strongly their participation to the formation of coordination bonds.[1] As a result, $Ln^{3+}$ exhibit sharp, atom-like emission bands ranging from the visible to the near-infrared (NIR) domains.[1] Additionally, lanthanide(III) ions boast other attractive luminescence properties, such as long luminescence lifetimes in comparison to organic fluorophores (microsecond to millisecond), emission bands the wavelengths of which are not affected by experimental conditions and enhanced resistance to photobleaching.[1,2] Such properties have triggered the interest for lanthanide(III)-containing compounds for applications in materials science as well as in biology for optical imaging or bioanalytical assays.[2–8] However, due to the symmetry forbidden nature of *f–f* transitions, most lanthanide(III) ions have extremely low molar absorption coefficients which affect negatively the number of corresponding emitted photons and detection sensitivity.[1] To overcome this major limitation, organic chromophoric ligands have been used for the complexation and sensitization of lanthanide(III) ions by a process called the "antenna effect".[9,10] In addition, another aspect that has to be considered for the design of luminescent lanthanide(III) molecular complexes is the proximity of C–H, O–H, and N–H bonds to the lanthanide(III) ions, as their vibrational overtones may couple with $Ln^{3+}$ excited states and quench emission through a non-radiative pathway.[11] Rare earth complexes have been designed that favor the sensitization either of lanthanide(III) ions emitting in the visible (for example, $Tb^{3+}$, $Dy^{3+}$, $Sm^{3+}$, $Eu^{3+}$) or in the NIR (for example, $Er^{3+}$, $Yb^{3+}$, $Nd^{3+}$).[12,13] Only for a few complexes has one type of antenna successfully sensitized both visible and NIR lanthanide(III) emissions.[14–19]

As single-ion magnets, lanthanide(III) ions have been of interest for applications in magnetic storage, quantum computing,[20] and spintronic devices,[21] thanks to their inherently large spin and magnetic anisotropies.[22,23] These properties are due to the unquenched orbital momentum and the strong spin-orbit coupling occurring in these metal ions. As a result, significant efforts have been directed to develop strategies to take advantage of lanthanide(III) intrinsic magnetic properties. It was shown that the control of the ligand field around lanthanide(III) ions has an important impact on their magnetic behavior. As examples, $Tb^{3+}$ complexes formed with phthalocyanine and lanthanide(III) polyoxometallates demonstrated how

[a] J. C. Lutter, Dr. J. W. Kampf, Prof. Dr. V. L. Pecoraro
Department of Chemistry
Willard H. Dow Laboratories
University of Michigan
Ann Arbor, MI 48109 (USA)
E-mail: vlpec@umich.edu

[b] Dr. S. V. Eliseeva, Prof. Dr. S. Petoud
Centre de Biophysique Moléculaire
CNRS UPR 4301, 45071 Orléans Cedex 2 (France)
E-mail: svetlana.eliseeva@cnrs.fr
stephane.petoud@inserm.fr

Supporting information and the ORCID identification number(s) for the author(s) of this article can be found under: https://doi.org/10.1002/chem.201801355.

the geometry of the ligand field influences the presence or absence of an easy-axis of magnetization.[24,25] Long and co-workers proposed that the ligand field will encourage an easy axis if the shapes of the lanthanide(III) orbitals are accommodated by the ligands, where the lanthanide(III) total orbital shape may be described as spherical ($Gd^{3+}$), oblate ($Dy^{3+}$, $Tb^{3+}$), or prolate ($Er^{3+}$, $Yb^{3+}$).[26] Ligand fields that are axially elongated promote an easy axis for oblate ions, while equatorially expanded ligand fields promote an easy-axis for prolate ions.[26]

Since their discovery in 1989,[27,28] metallacrowns, inorganic structural analogues to crown ethers, have demonstrated a high potential in numerous applications, including host-guest binding,[29–31] gas adsorption,[32] molecular magnetism,[33–38] and lanthanide(III)-based luminescence.[9,14,39] Metallacrowns possess a high degree of tunability based on the choice of ligand and metal, which uniquely allows for the predictable design of complexes towards a specific application.[40–44] For example, the use of closed shell cations such as gallium(III) and zinc(II) ions has led to the creation and characterization of lanthanide(III) MCs with record-breaking luminescence properties in molecular materials.[9,14] Metallacrowns have also established a rich history in molecular magnetism, both as 3d–4f bimetallic and as lanthanide(III) complexes. Examination of these systems has provided significant insight into the magnetic properties of 3d transition metals in association with lanthanide(III) ions. Herein, a new class of metallacrown-like structures is reported, $[LnGa_6(H_2shi)(Hshi)(shi)_7(C_5H_5N)]$ ($shi^{3-}$ = salicylhydroximate; Ln = Pr, Nd, Sm–Yb) in which the MC complexes resemble more the structures of cryptands rather than those of crown ethers while maintaining metallacrown-like [Metal-N-O] binding motifs. Metallacryptates have been described before, for example, a sandwich complex of two 12-$MC_{Ga^{III}N(shi)}$-4 complexes has been reported, which bound a sodium cation inside a cage like structure created by four $\mu_2$-hydroxides between $Ga^{III}$ ions of different metallacrowns.[45] In addition, another metallacryptate complex comprised of manganese and 2,2′-dipyridylketonediolate which encapsulates a manganese oxide core demonstrated interesting single-molecule magnetic properties.[46] This work presents the first example of metallacryptates with lanthanide(III)-based luminescence and magnetic slow relaxation obtained using the same scaffold.

## Results and Discussion

### Synthesis and structural analysis

The reaction between stoichiometric amounts of $H_3shi$ with lanthanide(III) and gallium(III) nitrate salts in presence of triethylamine results in the formation of complexes possessing the following composition, $[LnGa_6(H_2shi)(Hshi)(shi)_7(C_5H_5N)]$ ($shi^{3-}$ = salicylhydroximate; Ln = Pr, Nd, Sm–Yb), **Ln-1** (Scheme 1). The procedure outlined in Scheme 1 is similar to other gallium metallacrown synthetic routes, however, there are a few important distinctions that allow for the isolation of differing complexes. First, the metal to ligand stoichiometry (Ga:Ln:shi) is very important as a ratio of 4:1:4 results in a Ln[12-$MC_{Ga^{III}N(shi)}$-4] reported by Pecoraro and co-workers,[14] a

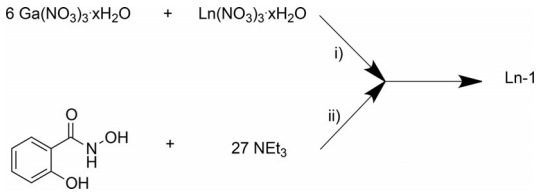


**Scheme 1.** Synthesis of $Ln^{III}/Ga^{III}$ [3.3.1] metallacryptate complexes, **Ln-1**: i) MeOH, ii) MeOH/pyridine.

2:1:4 ratio gives a $Ln_2Ga_4$ 16-MC-6 reported by Pecoraro, Mallah and co-workers,[37] and in the present case, a 6:1:9 ratio gives this metallacryptate. Although similar solvents are used, each reaction has a different solvent mixture. This difference in solvent composition alters the possible solubility and stability of each MC complex during the reaction. Lastly, it is possible that all three of these species co-exist to some extent in solution; however, the crystallization conditions for each complex differentiate which is most likely to crystallize. The 12-MC-4 and 16-MC-6 were slowly evaporated using different solvent conditions, while the metallacryptate was crystallized by slow diethyl ether diffusion. By applying these three tenets one may distinguish which complex is isolated reliably.

X-ray crystallographic data were obtained on single crystals of the terbium(III) analogue for the purpose of structural analysis (Figure 1). Powder X-ray diffraction shows that these complexes are isostructural within preferential orientation effects and varying degrees of crystallinity (Figure S2, Supporting Information). The central lanthanide(III) ion is nine-coordinate, with a geometry around it that most closely resembles a tricapped trigonal prism (see Figure S1, Supporting Information). Four of the gallium(III) ions (Ga2, Ga4, Ga5, and Ga6) are located in distorted octahedral environments with propeller conformations; Ga2 and Ga4 adopts a Λ chirality while Ga5 and Ga6

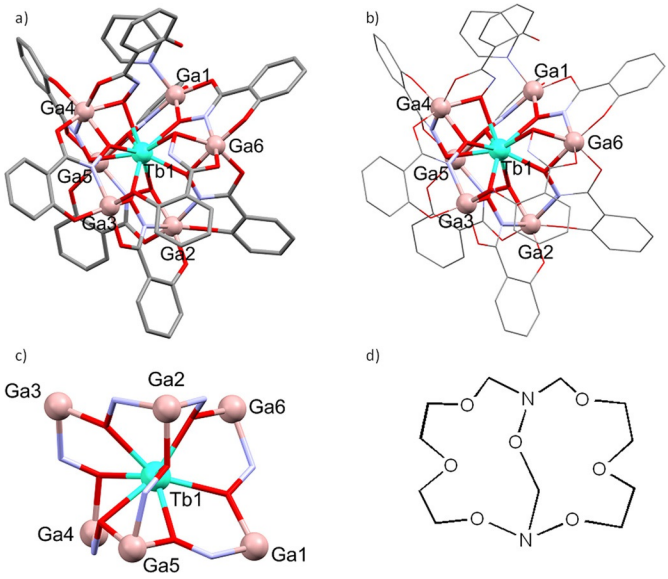


**Figure 1.** a) Representation of the structure of **Tb-1** obtained X-ray diffraction experiments on single crystals; b) highlight of the Ga-N-O motif; c) the metallacryptate core; d) complementary cryptand as a comparison.

adopt a Δ chirality. Such type of alternating absolute stereochemical isomerism has been reported for other metallacrowns.[47–49] The remaining gallium(III) ions (Ga1 and Ga3) are five coordinated, with a geometry closer to a square pyramid confirmed by Addison tau values which are closer to zero than one ($\tau = 0.2525$ and 0.2697, respectively; $\tau = (\alpha - \beta)/60$, in which $\alpha$ and $\beta$ are the two largest bond angles).[50]

Structurally similar to simpler metallacrowns, the described complexes also follow a binding motif that uses [M-N-O] repeating units. However, **Ln-1** complexes are not analogous to crown ethers but more closely resemble the structure of cryptands; for example, they can be compared to 1,10-diaza-2,5,8,12,15,18,20-heptaoxabicylco[8.8.2]icosane (Figure 1 d). On the basis of the cryptand nomenclature, the **Ln-1** complexes may be described as a $Ga^{III}$[3.3.1]metallacryptand, where Ga2 and Ga5 are considered to be analogous to the nitrogen atoms in a cryptand. With the adaptation of metallacryptand nomenclature defined by Saalfrank et al.[51] the shorthand is [Tb⊂{$Ga_6$(shi)$_7$}(Hshi)($H_2$shi)($C_5H_5N$)]($C_6H_{16}N$)$_3$. Inclusion of metallacrown style nomenclature gives the name [Tb⊂{[3.3.1.]20-$MC_{Ga^{III}N(shi)}$-7}(Hshi)($H_2$shi)($C_5H_5N$)]($C_6H_{16}N$)$_3$. The marriage of these nomenclatures describes the $Tb^{III}$ encapsulating $Ga^{III}$[3.3.1]metallacryptand structure very well in shorthand notation, which is useful for future structures of similar composition.

The central metal is the terbium(III) ion, while the six gallium(III) and seven of the $shi^{3-}$ ligands make up the metallacryptand. There are twenty atoms in the [Ga-N-O] motif, seven of which are oxygen atoms that are distributed across three "arms" in a 3:3:1 ratio. The remaining two $H_3$shi ligands bridge gallium(III) ions to the terbium(III). One $H_3$shi ligand is singly deprotonated ($H_2shi^-$) and bridges Ga4 to Tb1 in a "standing up" conformation while the other is doubly deprotonated ($Hshi^{2-}$) and bridges Ga3 and Ga6 to the Tb1 in a "laying down" conformation (Figure 1). There is a coordinated pyridine molecule on Ga1. Three triethylammonium cations provide the charge balance. Elemental analysis results, $^1$H NMR spectra of **La-1**, **Y-1** and **Lu-1**, consistent FT-IR spectra, and $[M+H]^{2-}$ peaks observed in ESI-MS spectra across the compounds prove the stoichiometry of the metallacryptate and confirm that it does not change across the lanthanide series (Figures S3, S4, and S5, Supporting Information).

One of the advantages of metallacrown complexes is the large degree of structural tunability that these species may tolerate. For example, the classic 12-MC-4 structure type has been synthesized using several trivalent metals of different natures, with varying bridging anions and with the ligand $shi^{3-}$ or one of its derivatives.[14,42,52] Because of the nature of the self-assembly process used for the synthesis of MCs, many *meta*-stable intermediates can be isolated upon modifications of the experimental conditions such as changing solvents or varying the nature of counter anions. These new species correspond to alternative, unpredicted structures or superstructures related to the classic MC archetype. Often, once these "serendipitous" molecules have been isolated, they can be prepared in a controlled way as they possess remarkable stability. One of these variants was reported by Lah et al. and described as a "metallacryptate" where three sodium(I) ions were bound to two 12-$MC_{Ga^{III}N(shi)}$-4 in a sandwich-like fashion, four $\mu_2$-hydroxide ions connecting the gallium(III) ions across the MC interface (Figure 2 a).[45] The coordination environments around $Ga^{III}$ ions are square pyramidal with the hydroximate ligands located in the plane and a bridging $\mu_2$-hydroxide located in the apical position. The central sodium ion is eight-coordinated with a square prismatic geometry while the two remaining sodium(I) ions present in the structure are seven-coordinated with a monocapped octahedral geometry. While this structure was initially described as a "metallacryptate", in retrospect, it is more reminiscent of an isolated clathrate unit of cubic structure. This system was also the first example of gallium(III) in a metallacrown assembly. However, the combination of gallium(III) and sodium(I) did not offer the opportunity for this complex to demonstrate molecular magnetism or other functional properties. Later, Dendrinou-Samara et al. reported another cage-like molecule that can be described as a metallacryptate based on manganese(II/III) cations, where the core of manganese(III) oxide/methoxide was encapsulated inside of the metallacryptand arms (Figure 2 b).[46] This structure was formed in situ by the conversion of 2,2′-dipyridylketonoxime into 2,2′-dipyridylketonediolate ($pdol^{2-}$) where four $Mn^{II}$, six $Mn^{III}$, 12 $pdol^{2-}$ and six azide ions made up the metallacryptand "arms". This structure can be deconstructed into the 16 Mn core and a 6-armed adamantoid metallacryptate. As shown in Figure 2 c,d, the topology of this molecule is close to an heteroadaman-

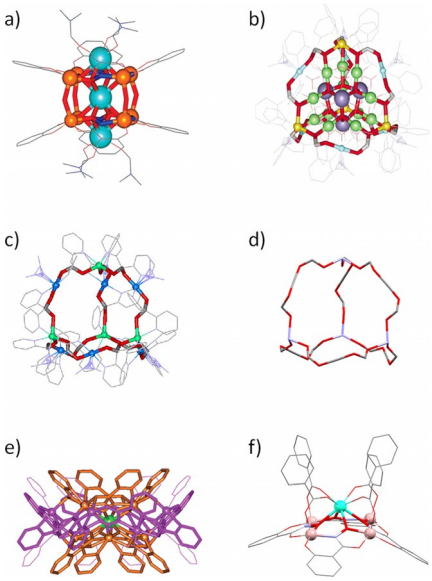


**Figure 2.** Previously described metallacrowns and metallacryptates. a) $Na_3$[12-$MC_{Ga^{III}N(shi)}$-4]$_2$$(OH)_4^-$.[45] b) $[Mn^{II}_4Mn^{III}_{22}(pdol)_{12}(\mu_2\text{-}OCH_3)_{12}(\mu_3\text{-}O)_{10}(\mu_4\text{-}O)_6(N_3)_6]^+$.[46] c) Representation of the metallacryptand topology with four capping $Mn^{II}$ ions and six linking $Mn^{III}$ ions with the MnO core removed for clarity. d) A representation of the metallacryptand is depicted as a hetero adamantane with propeller $Mn^{II}$ as nitrogen, $pdol^{2-}$ oxygens retained as oxygen atoms and all other atoms as carbon. e) $Tb^{III}$[12-MC-4]$_2$[24-MC-8]$^{3+}$.[39] f) Crystallographic representation of Dy(benzoate)$_4$[12-$MC_{Ga^{III}N(shi)}$-4].[14].

tane. This complex was characterized as a single molecule magnet. Subsequently, the perchlorate salt was isolated, which exhibited a slightly higher level of symmetry enhancing the SMM behavior. Fitting the frequency-dependent out-of-phase magnetic susceptibility to the Arrhenius equation yielded an effective energy barrier to magnetization relaxation, $U_{eff}$, of 11.5 $cm^{-1}$ for the azide complex and of 25.1 $cm^{-1}$ for the perchlorate complex.[53]

In 2011, Jankolovits, et al. created another interesting type of structure using zinc(II) and picolinic hydroximate ($picHA^{2-}$), which form an "encapsulated sandwich" topology that has similarities with $Na_3[12\text{-}MC_{Ga^{III}N(shi)}\text{-}4]_2(OH)_4$ (Figure 2e).[39,45] Here, two 12-MC-4 units encapsulate a lanthanide(III) cation instead of a sodium(I). The whole complex is stabilized by a larger 24-MC-8 ring, rather than by four $\mu_2$-hydoxides. The central lanthanide(III) is eight-coordinated in a square antiprism geometry while the zinc(II) atoms are five-coordinated in a square pyramidal geometry in the 12-MC-4s and octahedral within the 24-MC-8. This complex was not only fascinating from a structural point of view of supramolecular complexation, but it was the first example of a metallacrown complex to demonstrate the sensitization of characteristic NIR luminescence of ytterbium(III) and neodymium(III). Moreover recently, it has been shown that lanthanide(III)–zinc(II) MCs with an "encapsulated sandwich" topology assembled using pyrazine hydroximate ($pyzHA^{2-}$) are valuable agents for simultaneous cell fixation and staining as well as for NIR imaging of necrotic cells.[54–56]

The new gallium(III) [3.3.1] metallacryptand demonstrates an entirely different type of structure for the class of cage like metallacrowns. The metallacryptand binds a lanthanide(III) in a nine-coordinate tricapped trigonal prism environment (Figure S1, Supporting Information), utilizing only the $shi^{3-}$ ligands to form the structure. Unlike the previously reported gallium(III) 12-MC-4 structures from Lah et al. and Chow et. al. (Figure 2f),[14,45] this structure utilizes six gallium(III) in four octahedral sites that are in propeller conformations as well as two which are in square pyramidal coordination geometries. If one were to follow the path of Ga5-Ga4-Ga3-Ga2-Ga6-Ga1 through the Ga-N-O motif the geometries observed are Δ-octahedral, Λ-octahedral, square pyramidal, Λ-octahedral, Δ-octahedral, and square pyramidal. This kind of "alternating chirality" has been observed in other metallacrown complexes such as the ruffled manganese 15-MC-5 reported by Kessissoglou et. al.[47] This nine-coordinate lanthanide(III) geometry is also rarely observed in metallacrown-type structures, offering a unique opportunity to probe the possibility for single ion magnetism of lanthanide(III) ions in this environment. Because of the inclusion of nine $H_3$shi ligands into the lanthanide(III) coordination environment, the UV/Vis absorption due to the ligand-centered π–π* transitions should be larger than for the previously reported luminescent $Ln^{III}(benzoate)_4[12\text{-}MC_{Ga^{III}N(shi)}\text{-}4]$ that only contains four $shi^{3-}$ chromophores.[14] As the optically silent $Ga^{III}$ ion was used in the metallacryptand, and $shi^{3-}$ is known to sensitize a large diversity of lanthanide(III) ions of different nature.[14] Therefore, **Ln-1** show a strong potential to exhibit attractive emission properties.

## Photophysical properties

### *Ligand-centered photophysical properties*

Absorption and diffuse reflectance spectra of the ligand $H_3$shi and **Ln-1** complexes are given in Supporting Information (Figures S6 and S7). In methanol, the ligand $H_3$shi exhibits several bands due to π*←π transitions with the lowest energy one centered at ~300 nm ($\varepsilon = 3.9\times10^3\ M^{-1}cm^{-1}$). The formation of **Ln-1** metallacryptate leads to a redshift of these absorption bands and to an increase of the molar absorption coefficients, which is directly proportional to the number of $H_3$shi ligands present in the molecule ($\varepsilon_{Gd\text{-}1} = 4.5\times10^4\ M^{-1}cm^{-1}$ at 310 nm). The energy position of the singlet state was estimated from the edge of absorption spectra of **Ln-1** complexes and found to be located at energies of 29410 $cm^{-1}$ (340 nm). Diffuse reflectance spectra recorded on solid state samples of **Ln-1** exhibit similar broad bands in the range of 200–380 nm except for the **Eu-1** metallacryptate where an extension of the band towards lower energies (up to 470 nm) was observed. In addition, in the reflectance spectra of all **Ln-1** except for **Eu-1** and **Tb-1**, narrow bands in the visible and the NIR ranges were observed which could be assigned to the *f–f* transitions belonging to the corresponding lanthanide(III) ions.

To estimate position of the triplet state in **Ln-1** complexes, the phosphorescence spectrum of the **Gd-1** complex was measured in the solid state at 77 K. Upon excitation at 350 nm with a flash Xenon lamp and application of a 100 μs delay after the excitation flash, **Gd-1** revealed the presence of a broad-band emission in the range 430–750 nm (Figure 3, black trace). A Gaussian deconvolution of the collected phosphorescence spectrum (Figure 3, coloured traces) allowed to estimate the position of the triplet state ($T_1$) as a 0–0 transition, 21600 $cm^{-1}$ (463 nm).

The energy positions of the ligand-centered excited states, in particular $S_1$ and $T_1$, with respect to the $Ln^{3+}$ resonance accepting levels, are crucial for the rationalization of luminescent lanthanide(III)-based complexes and materials, controlling rates of different energy transfer steps and, as a consequence, global photophysical parameters. The triplet state is considered to be one of the major feeding levels for $Ln^{3+}$ while

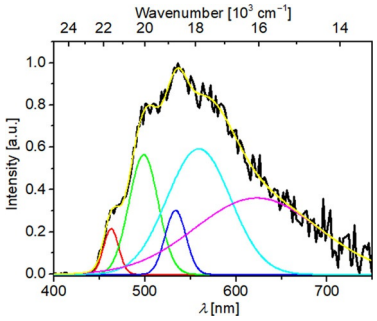


**Figure 3.** Phosphorescence spectrum (black trace) recorded for **Gd-1** at 77 K in the solid state upon excitation at 350 nm and applying a 100 μs delay after the excitation flash. Coloured traces represent the individual Gaussian spectra obtained from the deconvolution of the experimental phosphorescence spectrum.

$\Delta E(S_1-T_1)$ is affecting the efficiency of intersystem crossing. Thus, the energy of the $S_1$ electronic state in **Ln-1** complexes was found to be located at 29410 $cm^{-1}$, while that of $T_1$ at 21 600 $cm^{-1}$ giving an energy difference of 7810 $cm^{-1}$. The latter value is greater than 5000 $cm^{-1}$, which is often regarded as a benchmark for efficient intersystem crossing. In general, the $T_1$ level is located higher in energy than the main emissive states of $Ln^{3+}$ which range from 21350 $cm^{-1}$ for $Tm^{3+}$ to 6700 $cm^{-1}$ for $Er^{3+}$.[57,58] Compared to the previously reported $Ga^{3+}/Ln^{3+}$ metallacrowns, the core of which is also assembled from $H_3$shi ligands, singlet and triplet states in **Ln-1** metallacryptates are lower in energy by 440 and 570 $cm^{-1}$, respectively.[14] This difference is small but can be significantly detrimental to the sensitization of some $Ln^{3+}$, like $Tm^{3+}$, $Dy^{3+}$ and $Tb^{3+}$ that possess emissive energy levels located too close to the $T_1$ energy level that increases the probability of back energy transfer processes from $Ln^{3+}$ levels, that is, $^1G_4$ (21350 $cm^{-1}$), $^4F_{9/2}$ (21100 $cm^{-1}$) and $^5D_4$ (20400 $cm^{-1}$),[57,58] to those located on the ligands.

### *Lanthanide(III)-centered photophysical properties*

The examination of the photophysical properties of **Ln-1** complexes in the solid state at room temperature demonstrated that a wide range of lanthanide(III) ions are sensitized by the gallium(III) [3.3.1] metallacryptate scaffold through antenna effect (Figure 4). The characteristic emission in the visible

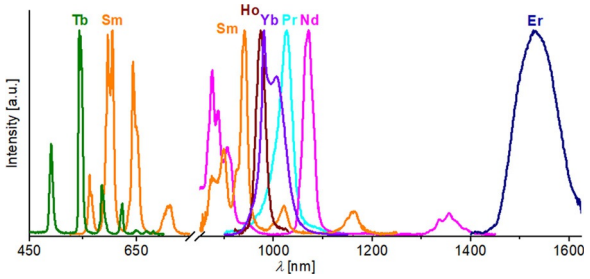


**Figure 4.** Corrected and normalized emission spectra of **Ln-1** complexes measured in the solid state upon excitation at 350 nm at room temperature.

range arising from $Tb^{3+}$, in the NIR range resulting from $Pr^{3+}$, $Nd^{3+}$, $Ho^{3+}$, $Er^{3+}$, and $Yb^{3+}$, as well as $Sm^{3+}$ in both the visible and the NIR ranges, could be observed for **Ln-1** metallacryptates upon excitation into the ligand-centered levels in the 300–350 nm range. On the other hand, $Tm^{3+}$ and $Dy^{3+}$ emissions were not observed in **Ln-1**. This can be traced back to the low energy position of the $T_1$ level in metallacryptates that increases the probability of back energy transfer $T_1 \leftarrow Ln^{3+}$. $Eu^{3+}$ emission was also not detected in **Eu-1** which is most probably caused by a quenching effect induced by the formation of ligand-to-metal charge transfer (LMCT) states. The presence of a LMCT is reflected by the broadening and the red-shifting of the diffuse reflectance band in **Eu-1** complexes compared to these of the other **Ln-1** (Figure S7, Supporting Information). Excitation spectra of **Ln-1** collected upon monitoring the emission of $Ln^{3+}$ at 1025 ($Pr^{3+}$), 1067 ($Nd^{3+}$), 600 ($Sm^{3+}$), 545 ($Tb^{3+}$), 875 ($Ho^{3+}$), 1525 ($Er^{3+}$) and 980 ($Yb^{3+}$) nm revealed the presence of broad bands in the UV/Visible spectral domain (up to 400 nm) (Figure 5). The similarity between the shapes of these excitation spectra measured on metallacryptates containing lanthanide(III) cations of different natures and their widths at half height confirm that $Ln^{3+}$ are sensitized

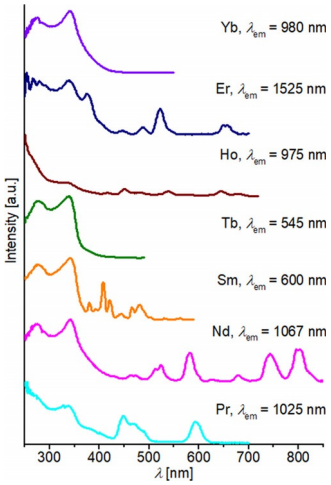


**Figure 5.** Corrected and normalized excitation spectra of **Ln-1** complexes in the solid state recorded upon monitoring the main transitions ($\lambda_{em}$) of the corresponding $Ln^{III}$ ions at room temperature.

through the antenna effect, that is an energy transfer from the chromophoric ligands. The presence of sharper bands corresponding to the *f–f* transitions in the excitation spectra of **Ln-1** metallacryptates reflects the additional possibility of direct excitation of some of the lanthanide(III) ions (Figure 5). Quantitative photophysical parameters, quantum yields upon ligand excitation ($Q^L_{Ln}$) and luminescence lifetimes ($\tau_{obs}$) of **Ln-1** in the solid state are summarized in Table 1.

In the case of $Nd^{III}$ and $Er^{III}$ metallacryptates intrinsic quantum yields ($Q^{Ln}_{Ln}$) under direct excitation of the lanthanide(III)

**Table 1.** Photophysical parameters of **Ln-1** in the solid state.[a]

| Ln-1[a] | $\Delta E$ [$cm^{-1}$][b] | $\tau_{obs}$ [μs][c] | $Q^L_{Ln}$ [%][d] |
|---|---|---|---|
| Pr | 4760 | 0.063(1) | $3.7(2)\times10^{-3}$ |
| Nd | 10140 | 0.71(1) | $1.71(5)\times10^{-1}$ |
| Sm | 3700 | 70(1) | 1.70(9)[e] |
| Tb | 1200 | 20.7(5):71% 4.54(6):29% | $1.89(3)\times10^{-1}$ |
| Ho | 6100 | 0.037(1) | $1.1(2)\times10^{-3}$ |
| Er | 14900 | 0.905(8) | $7.1(2)\times10^{-3}$ |
| Yb | 11300 | 7.26(2) | 0.65(3) |

[a] Collected at room temperature, $2\sigma$ values are given between parentheses, relative errors: $\tau_{obs}$, ±2%; $Q^L_{Ln}$, ±10%. [b] $\Delta E(T_1\text{-}E^{Ln})$ is the energy difference between $Ln^{3+}$ emissive state and the ligand-centered triplet state energy $T_1 = 21\ 600\ cm^{-1}$: $E^{Pr}(^1D_2) = 16{,}840\ cm^{-1}$, $E^{Nd}(^4F_{3/2}) = 11{,}460\ cm^{-1}$, $E^{Sm}(^4G_{5/2}) = 17{,}900\ cm^{-1}$, $E^{Tb}(^4D_4) = 20{,}400\ cm^{-1}$, $E^{Ho}(^5F_5) = 15{,}500\ cm^{-1}$, $E^{Er}(^4I_{13/2}) = 6{,}700\ cm^{-1}$, and $E^{Yb}(^2F_{5/2}) = 10{,}300\ cm^{-1}$.[57,58] [c] $\lambda_{ex} = 355$ nm. [d] $\lambda_{ex} = 350$ nm. [e] Total quantum yield. Partial $Q^L_{Sm}$ in the visible range (500–750 nm) equal to 1.64(9) % and in the NIR range (850-1250 nm) to 0.055(2) %.

ions at 750 and 650 nm, respectively, could be measured and found to be 0.150(4) and 1.2(1)×10$^{-2}$%. These values allowed us to estimate the sensitization efficiencies ($\eta_{sens}$) of the metallacryptate scaffold, defined as $Q^{L}_{Ln}/Q^{Ln}_{Ln}$, for **Nd-1** (≈100%) and **Er-1** (59(13)%). Despite high sensitization efficiencies demonstrated for $Nd^{III}$ and $Er^{III}$ metallacryptates, in general, $Q^{L}_{Ln}$ and $\tau_{obs}$ are significantly lower for **Ln-1** ($Ln^{3+}$ = Nd, Sm, Tb, Ho, Er, Yb) metallacryptates compared to the corresponding $Ln^{III}(benzoate)_4$[12-MC-4] metallacrowns previously reported (Table S1, Supporting Information).[14] Such behavior can be probably attributed to the proximity of N–H and C–H oscillators (≈3.2–3.5 Å) on the protonated $H_3$shi ligands that bridge $Ln^{3+}$ to the metallacryptate scaffold, vibrational overtones of which may couple with the excited states of the lanthanide(III) ions leading to their depopulation. Moreover, back energy transfer processes are also likely responsible for the modest luminescence performance of the $Tb^{3+}$ in metallacryptates in which the energy difference $\Delta E(T_1-{}^5D_4)$ is only 1200 cm$^{-1}$, in comparison with the $Tb^{III}(benzoate)_4$[12-MC-4] metallacrown ($Q^{L}_{Tb}$: 1.89(3).10$^{-1}$ vs. 34.7(1) %, $\tau_{obs}$: 19.4(5) vs. 1080(10) μs; Table S1, Supporting Information).

### Magnetic behavior

Magnetic characterization of the $Ga^{III}$[3.3.1]metallacryptate complexes revealed slow relaxation from AC susceptibility experiments for **Nd-1**, **Dy-1**, and **Yb-1**. However, only **Dy-1** displays an out of phase susceptibility without the presence of an applied DC field (Figure S11 Supporting Information) indicating enhanced slow relaxation due to a quenching effect of quantum tunneling of magnetization (QTM), and an Orbach relaxation. **Nd-1** and **Yb-1** show no signs of slow relaxation in absence of an applied field, and do not change the maximum frequency as a function of DC field strength (Figure S12, Supporting Information). Based on these observations, **Dy-1** was characterized more rigorously as a single-ion magnet.

Temperature dependent DC $\chi_m$T was measured using a field of 2000 Oe from 2 K to 300 K (Figure S9, Supporting Information), reaching a value of 13.48 cm$^3$·K mol$^{-1}$ at 300 K, which is lower than theoretical values for a single non-interacting $Dy^{3+}$ ion (14.17 cm$^3$·K mol$^{-1}$, $^6H_{15/2}$, $S=5/2$, $L=5$, $g=4/3$, $J=15/2$). This result may be explained by long range antiferromagnetic interactions.[22] The $\chi_mT$ decreases steadily with cooling to a minimal value of 9.18 cm$^3$·K mol$^{-1}$ at 2 K, which is likely due to a depopulation of ground $J$ sublevels or to an intermolecular antiferromagnetic interaction.[59–61] Isothermal magnetization at 2 K from 0 T to 7 T (Figure S10, Supporting Information) increases to a saturation value of 5.55 Nβ, which is lower than theoretical values observed for a single $Dy^{3+}$ ion (10 Nβ), likely due to the presence of low lying excited states and crystal field influence.[62,63]

To probe the molecular environment of the **Dy-1** complex, Cole–Cole plots (Figure 6b) from 2 to 4 K were fitted using [Equations (1) and (2)].[64]

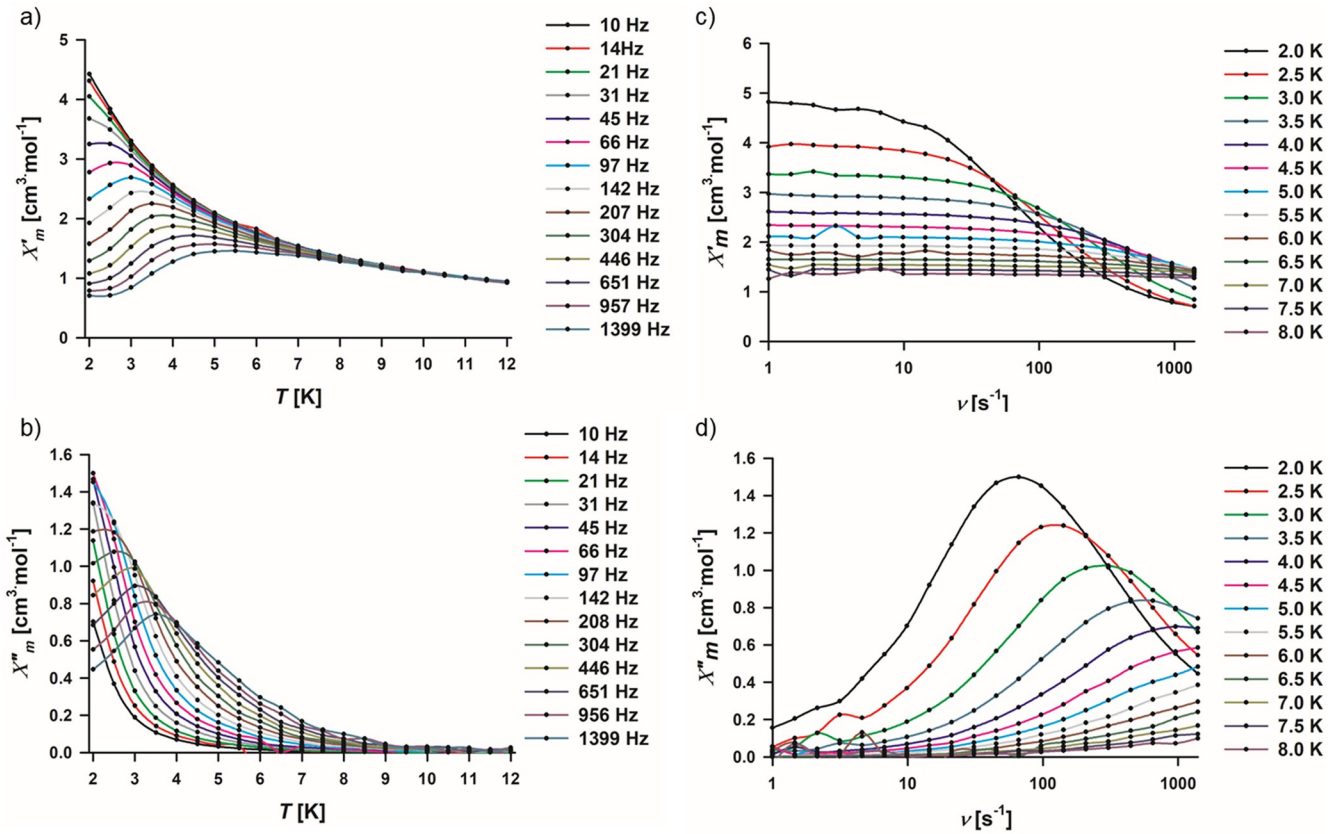


**Figure 6.** AC susceptibility of **Dy-1**; a) in phase temperature dependent curves; b) out of phase temperature dependent curves; c) in phase frequency dependent curves; d) out of phase frequency dependent curves, under an applied field of 750 Oe. Solid lines are plotted as a guide for the eye.

$$\chi'_m(\omega) = \chi s + \frac{(\chi_T - \chi_S)\left[1 + (\omega\tau)^{(1-\alpha)}\sin\left(\frac{\alpha\pi}{2}\right)\right]}{1 + 2(\omega\tau)^{(1-\alpha)}\sin\left(\frac{\alpha\pi}{2}\right) + (\omega\tau)^{2(1-\alpha)}} \quad (1)$$

$$\chi''_m(\omega) = \frac{(\chi_T - \chi_S)\left[(\omega\tau)^{(1-\alpha)}\cos\left(\frac{\alpha\pi}{2}\right)\right]}{1 + 2(\omega\tau)^{(1-\alpha)}\sin\left(\frac{\alpha\pi}{2}\right) + (\omega\tau)^{2(1-\alpha)}} \quad (2)$$

in which $\chi_S$ is the adiabatic susceptibility, $\chi_T$ is the isothermal susceptibility, $\omega$ is the angular frequency, $\tau$ is the magnetic relaxation time, and $\alpha$ is a parameter constrained between 0 and 1 which describes the relative range of distributions. Fits gave a range of $\alpha = 0.2041–0.2790$ (Table S2, Supporting Information), which suggests that there is a small distribution of molecular environments. The semicircular shape indicates that there is one barrier of relaxation, and the symmetrical shape indicates that only one species is present.

Variable temperature and variable frequency AC susceptibility was collected with an AC field of 3 Oe, and applied DC fields of 0 Oe (Figure S11, Supporting Information) and 750 Oe to suppress the QTM (Figure 7). The small 750 Oe applied field

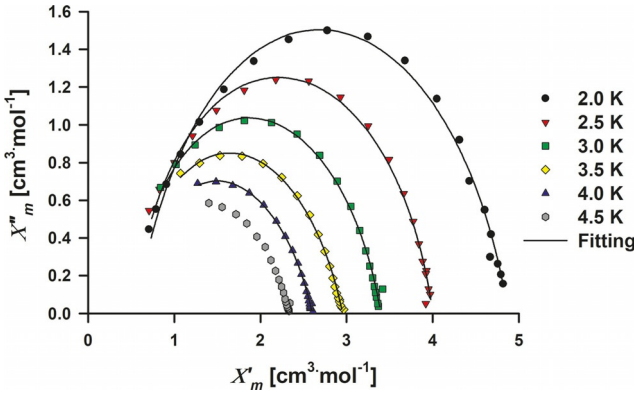


**Figure 7.** Cole–Cole plot of **Dy-1**, black line represents the fit using [Eqs. (1) and (2)].

selection is described in the supplemental information (Figure S13, Supporting Information). In a 0 Oe applied field, the χ"m increases slightly at temperatures below 10 K, but no peak maxima are present, a prevalent observation of lanthanide SIMs.[24,61,65–67] However, under the 750 Oe applied field, the χ"m signal rises significantly between 7–9 K and peak maxima were observable due to the suppression of QTM. Fitting the temperature dependent data from 208 to 1399 Hz to a Lorenzian function $\left(\chi''_m = a/(1 + ((T - T_0)/b)^2)\right)$ allowed for the generation of an Arrhenius plot (Figure 8), which was fit to the Arrhenius Law ($\ln(1/\tau) = \ln(1/\tau_0) - U_{eff}/k_B \cdot T$). This operation resulted in evidence for a pre-exponential term of $\tau_0 = 3.6 \times 10^{-6}$ s$^{-1}$ and an effective barrier ($U_{eff}$) of 12.7 K, confirming field enhanced magnetic slow relaxation.

Work by Lannes and Luneau show similar phenomena for slow magnetization relaxations in nine-coordinate tricapped-trigonal prism dysprosium(III) and ytterbium(III) complexes, $[Ln(Tpz)_2Bpz]\cdot xCH_2Cl_2$.[66] Based on crystal-field calculations of the pyrazolyl borates it was determined that the relaxation of

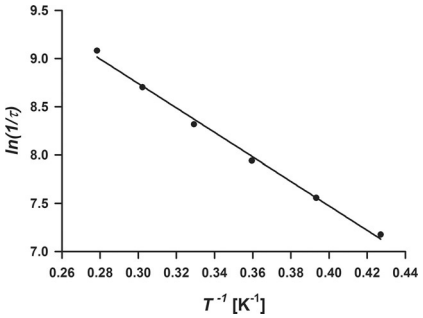


**Figure 8.** Arrhenius plot of **Dy-1**, derived from temperature dependent $\chi''_m$, the blue line represents the best fit to the Arrhenius law.

the $Dy^{III}$ in $[Dy(Tpz)_2Bpz]\cdot xCH_2Cl_2$ was consistent with a thermally driven Orbach process, while the one of the $Yb^{III}$ ion was better described by a Raman process, rendering any effective barrier to magnetization relaxation an artifact of the applied field.[66] In addition, tris-oxydiacetate complexes of dysprosium(III) and erbium(III) were characterized by Coronado and co-workers.[68] In this case the $Dy^{III}$ and $Er^{III}$ complexes demonstrated frequency dependent χ" responses both in the presence and absence of an applied 1000 Oe field. However, the $Dy^{III}$ analogue was not strong enough to show peak maxima above 2 K, while the $Er^{III}$ complex was determined to have a barrier of 46 K. Our findings are consistent with Lannes and Luneau's work, where both prolate and oblate lanthanide(III) ions showed slow magnetic relaxation in a nine-coordinate environment. The prolate $Yb^{III}$ ion and intermediate $Nd^{III}$ ion did display similar behavior, given that the field strength did not change the frequency of the relaxation, suggesting that like the pyrazolyl borate complex, these ions likely follow Raman processes with artificial relaxation barriers from the applied field. The oblate $Dy^{III}$ ion, however, does show a true thermal barrier to relaxation, with a value that is roughly half of that observed for the pyrazolyl borates ($U_{eff} = 20.3$ vs. 12.7 K), which may be explained by differences in the ligand field. However, the oblate $Dy^{III}$ showed a larger barrier to relaxation than the corresponding tris-oxydiacetate. The observation of slow relaxation of $Nd^{III}$ ion in single-ion complexes of nine-coordinate geometry is somewhat rare, and has only been observed in one other complex reported by Coronado and co-workers, which was also based on pyrazolyl borates.[69] Unlike the tris-oxydiacetate complexes, $Er^{III}$ did not display slow relaxation as the [3.3.1]metallacryptate. The differences in this behavior is likely due to the variation of the ligand field geometry between the metallacryptate and the tris-oxydiacetates where in the former $Ln^{III}$ ion is located in a distorted tricapped trigonal prism environment, while in the latter the true tricapped trigonal prism with $D_3$ symmetry has been observed.[25,26]

## Conclusion

A new class of coordination compounds was discovered here which, like metallacrowns, contains a [M-N-O] repeating motif resulting from the coordination of gallium(III) metal ions to sal-

icylhydroximate ligands. These compounds are reminiscent of cryptates, and are best described as lanthanide(III) complexes of a gallium(III) [3.3.1] metallacryptand which are able to bind lanthanide(III) ions of different natures from praseodymium(III) to ytterbium(III), with the exception of the radioactive promethium which was not studied. Characteristic lanthanide(III)-based luminescence was observed in the solid state in either the visible, or the NIR ranges, or in both domains, for $Tb^{III}$, or $Pr^{III}$, $Nd^{III}$, $Ho^{III}$, $Er^{III}$, $Yb^{III}$, or $Sm^{III}$ [3.3.1] metallacryptates, respectively, upon excitation into the ligand-centered levels in the range 300–350 nm. A larger number of $H_3$shi ligands present in the metallacryptates compared to the $Ln^{III}(benzoate)_4$[12-MC-4] metallacrowns[14] (nine vs. four) is responsible for higher molar absorption coefficients observed for the former one. However the quantum yields of metallacryptates are diminished due to the quenching induced by the overtones of N–H and C–H bonds located on the ligand. A slow magnetization relaxation was observed for $Nd^{III}$, $Dy^{III}$ and $Yb^{III}$ $Ga^{III}$[3.3.1] metallacryptates. Dysprosium(III) analogue demonstrated an Orbach relaxation with an effective barrier of 12.7 K, while neodymium(III) and ytterbium(III) metallacryptates likely follow Raman processes with artificial, field-induced barriers of relaxation. A combined study of luminescent and magnetic properties could provide a path for a deeper level of understanding of lanthanide(III) electronic structure and further discoveries, while metallacrowns and metallacryptates may be considered as ideal scaffolds to apply such strategy.

## Experimental Section

**Synthetic materials**: Gallium(III) nitrate hydrate (Sigma Aldrich, 99%), praseodymium(III) nitrate hexahydrate (Sigma Aldrich, 99.9%), neodymium(III) nitrate hexahydrate (Sigma Aldrich, 99.9%), samarium(III) nitrate hexahydrate (Sigma Aldrich, 99.9%), europium(III) nitrate hexahydrate (Sigma Aldrich, 99.9%), gadolinium(III) nitrate hexahydrate (Alfa, Aesar, 99.9%), terbium(III) nitrate pentahydrate (Sigma Aldrich, 99.9%), dysprosium(III) nitrate pentahydrate (Alfa Aesar, 99.9%), holmium(III) nitrate pentahydrate(Sigma Aldrich, 99.9%), thulium(III) nitrate hydrate (Sigma Aldrich, 99.9%), erbium(III) nitrate pentahydrate (Sigma Aldrich, 99.9%), ytterbium nitrate (Sigma Aldrich, 99.9%), salicylhydroxamic acid (Alfa Aesar, 99%), methanol (Fischer, ACS grade), pyridine (Fisher, ACS grade), and triethylamine (Acros, 99%). All reagents were used as received without further purification.

*General synthetic procedure for Ln⊂{[3.3.1] 20-$MC_{Ga^{III}N(shi)}$-7} complexes*: The lanthanide(III) nitrate hydrate (0.167 mmol) and gallium(III) nitrate hydrate (1 mmol) salts were mixed in 10 mL of methanol, resulting in the formation of a clear and colorless solution. Separately, salicylhydroxamic acid (1.5 mmol) and triethylamine (4.5 mmol) were mixed in 10 mL of methanol, followed by an addition of 10 mL of pyridine, resulting in a clear and colorless solution. The solutions were mixed, resulting in the observation of a white precipitate and colorless gas evolved briefly. After several minutes the solution returns to a clear and colorless state and was stirred for one hour, then filtered. Diffusion of diethyl ether into the filtrate afforded pure powder or needle product in periods of time from one to three weeks. Isolated product was dried under vacuum pressure of approximately 100 mTorr.

*$[PrGa_6(H_2shi)(Hshi)(shi)_7(HNEt_3)_3(C_5H_5N)]\cdot C_5H_5N\cdot 4H_2O$*, **Pr-1**: The synthetic yield was 28% based on praseodymium nitrate hexahydrate. Selected IR peaks (Diamond ATR): $\tilde{\nu}=1654\ cm^{-1}$, $1604\ cm^{-1}$, $1575\ cm^{-1}$, $1525\ cm^{-1}$, $1473\ cm^{-1}$, $1444\ cm^{-1}$, $1391\ cm^{-1}$. $1314\ cm^{-1}$, $1267\ cm^{-1}$, $1154\ cm^{-1}$, $1100\ cm^{-1}$, $1025\ cm^{-1}$, $945\ cm^{-1}$, $920\ cm^{-1}$, $860\ cm^{-1}$, $757\ cm^{-1}$, $672\ cm^{-1}$, $602\ cm^{-1}$. ESI-MS (180 V), calculated $PrGa_6C_{63}H_{40}N_9O_{27}$ $[M+H]^{2-}$: 957.33, found 956.33. Elemental analysis of $PrGa_6C_{91}H_{105}N_{14}O_{31}$ [fw = 2450.15 g mol$^{-1}$] calcd (%): C 44.61, H 4.32, N 8.00; found: C 44.98, H 4.28, N 8.22.

*$[NdGa_6(H_2shi)(Hshi)(shi)_7(HNEt_3)_3(C_5H_5N)]\cdot C_5H_5N\cdot 7H_2O$*, **Nd-1**: The synthetic yield was 2% based on neodymium nitrate hexahydrate. Selected IR peaks (Diamond ATR): $\tilde{\nu}=1654\ cm^{-1}$, $1604\ cm^{-1}$, $1575\ cm^{-1}$, $1525\ cm^{-1}$, $1473\ cm^{-1}$, $1444\ cm^{-1}$, $1391\ cm^{-1}$. $1314\ cm^{-1}$, $1267\ cm^{-1}$, $1154\ cm^{-1}$, $1100\ cm^{-1}$, $1025\ cm^{-1}$, $945\ cm^{-1}$, $920\ cm^{-1}$, $860\ cm^{-1}$, $757\ cm^{-1}$, $672\ cm^{-1}$, $602\ cm^{-1}$. ESI-MS (180 V), calculated $NdGa_6C_{63}H_{40}N_9O_{27}$ $[M+H]^{2-}$: 957.33, found 956.33. ESI-MS (180 V), calculated $NdGa_6C_{63}H_{40}N_9O_{27}$ $[M+H]^{2-}$: 956.83, found 958.83. Elemental analysis of $NdGa_6C_{91}H_{111}N_{14}O_{34}$ [fw = 2507.53 g mol$^{-1}$] calcd (%): C 43.59, H 4.46, N 7.82; found: C 43.59, H 4.30, N 7.87.

*$[SmGa_6(H_2shi)(Hshi)(shi)_7(HNEt_3)_3(C_5H_5N)]\cdot C_5H_5N\cdot 6H_2O$*, **Sm-1**: The synthetic yield was 33% based on samarium nitrate hexahydrate. Selected IR peaks (Diamond ATR): $\tilde{\nu}=1654\ cm^{-1}$, $1604\ cm^{-1}$, $1575\ cm^{-1}$, $1525\ cm^{-1}$, $1473\ cm^{-1}$, $1444\ cm^{-1}$, $1391\ cm^{-1}$. $1314\ cm^{-1}$, $1267\ cm^{-1}$, $1154\ cm^{-1}$, $1100\ cm^{-1}$, $1025\ cm^{-1}$, $945\ cm^{-1}$, $920\ cm^{-1}$, $860\ cm^{-1}$, $757\ cm^{-1}$, $672\ cm^{-1}$, $602\ cm^{-1}$. ESI-MS (180 V), calculated $SmGa_6C_{63}H_{40}N_9O_{27}$ $[M+H]^{2-}$: 957.33, found 956.33. ESI-MS (180 V), calculated $SmGa_6C_{63}H_{40}N_9O_{27}$ $[M+H]^{2-}$: 961.84, found 961.84. Elemental analysis of $SmGa_6C_{91}H_{109}N_{14}O_{33}$ [fw = 2495.64 g mol$^{-1}$] calcd (%): C 43.80, H 4.40, N 7.86; found: C 43.81, H 4.32, N 8.00.

*$[EuGa_6(H_2shi)(Hshi)(shi)_7(HNEt_3)_3(C_5H_5N)]\cdot C_5H_5N\cdot 3H_2O$*, **Eu-1**: The synthetic yield was 12% based on europium nitrate hexahydrate. Selected IR peaks (Diamond ATR): $\tilde{\nu}=1654\ cm^{-1}$, $1604\ cm^{-1}$, $1575\ cm^{-1}$, $1525\ cm^{-1}$, $1473\ cm^{-1}$, $1444\ cm^{-1}$, $1391\ cm^{-1}$. $1314\ cm^{-1}$, $1267\ cm^{-1}$, $1154\ cm^{-1}$, $1100\ cm^{-1}$, $1025\ cm^{-1}$, $945\ cm^{-1}$, $920\ cm^{-1}$, $860\ cm^{-1}$, $757\ cm^{-1}$, $672\ cm^{-1}$, $602\ cm^{-1}$. ESI-MS (180 V), calculated $EuGa_6C_{63}H_{40}N_9O_{27}$ $[M+H]^{2-}$: 957.33, found 956.33. ESI-MS (180 V), calculated $EuGa_6C_{63}H_{40}N_9O_{27}$ $[M+H]^{2-}$: 962.84, found 962.34. Elemental analysis of $EuGa_6C_{91}H_{103}N_{14}O_{30}$ [fw = 2443.19 g mol$^{-1}$] calcd (%): C 44.74, H 4.25, N 8.03; found: C 44.62, H 4.18, N 8.17.

*$[GdGa_6(H_2shi)(Hshi)(shi)_7(HNEt_3)_3(C_5H_5N)]\cdot C_5H_5N\cdot 5H_2O$*, **Gd-1**: The synthetic yield was 46% based on gadolinium nitrate hexahydrate. Selected IR peaks (Diamond ATR): $\tilde{\nu}=1654\ cm^{-1}$, $1604\ cm^{-1}$, $1575\ cm^{-1}$, $1525\ cm^{-1}$, $1473\ cm^{-1}$, $1444\ cm^{-1}$, $1391\ cm^{-1}$. $1314\ cm^{-1}$, $1267\ cm^{-1}$, $1154\ cm^{-1}$, $1100\ cm^{-1}$, $1025\ cm^{-1}$, $945\ cm^{-1}$, $920\ cm^{-1}$, $860\ cm^{-1}$, $757\ cm^{-1}$, $672\ cm^{-1}$, $602\ cm^{-1}$. ESI-MS (180 V), calculated $GdGa_6C_{63}H_{40}N_9O_{27}$ $[M+H]^{2-}$: 957.33, found 956.33. ESI-MS (180 V), calculated $GdGa_6C_{63}H_{40}N_9O_{27}$ $[M+H]^{2-}$: 964.84, found 964.84. Elemental analysis of $GdGa_6C_{91}H_{107}N_{14}O_{32}$ [fw = 2484.51 g mol$^{-1}$] calcd (%): C 43.91, H 4.39, N 7.89; found: C 43.98, H 4.44, N 8.27.

*$[TbGa_6(H_2shi)(Hshi)(shi)_7(HNEt_3)_3(C_5H_5N)]\cdot C_5H_5N\cdot H_2O$*, **Tb-1**: The synthetic yield was 36% based on terbium nitrate pentahydrate. Selected IR peaks (Diamond ATR): $\tilde{\nu}=1654\ cm^{-1}$, $1604\ cm^{-1}$, $1575\ cm^{-1}$, $1525\ cm^{-1}$, $1473\ cm^{-1}$, $1444\ cm^{-1}$, $1391\ cm^{-1}$. $1314\ cm^{-1}$, $1267\ cm^{-1}$, $1154\ cm^{-1}$, $1100\ cm^{-1}$, $1025\ cm^{-1}$, $945\ cm^{-1}$, $920\ cm^{-1}$, $860\ cm^{-1}$, $757\ cm^{-1}$, $672\ cm^{-1}$, $602\ cm^{-1}$. ESI-MS (180 V), calculated $TbGa_6C_{63}H_{40}N_9O_{27}$ $[M+H]^{2-}$: 957.33, found 956.33. ESI-MS (180 V), calculated $TbGa_6C_{63}H_{40}N_9O_{27}$ $[M+H]^{2-}$: 966.34, found 966.34. Elemental analysis of $TbGa_6C_{91}H_{99}N_{14}O_{28}$ [fw = 2414.13 g mol$^{-1}$] calcd (%): C 45.28, H 4.13, N 8.12; found: C 45.43, H 4.23, N 8.19.

*$[DyGa_6(H_2shi)(Hshi)(shi)_7(HNEt_3)_3(C_5H_5N)]\cdot 6H_2O$*, **Dy-1**: The synthetic yield was 24% based on dysprosium nitrate pentahydrate. Selected IR peaks (Diamond ATR): $\tilde{\nu}=1654\ cm^{-1}$, $1604\ cm^{-1}$, $1575\ cm^{-1}$, $1525\ cm^{-1}$, $1473\ cm^{-1}$, $1444\ cm^{-1}$, $1391\ cm^{-1}$. $1314\ cm^{-1}$,

1267 $cm^{-1}$, 1154 $cm^{-1}$, 1100 $cm^{-1}$, 1025 $cm^{-1}$, 945 $cm^{-1}$, 920 $cm^{-1}$, 860 $cm^{-1}$, 757 $cm^{-1}$, 672 $cm^{-1}$, 602 $cm^{-1}$. ESI-MS (180 V), calculated $DyGa_6C_{63}H_{40}N_9O_{27}$ $[M+H]^{2-}$: 957.33, found 956.33. ESI-MS (180 V), calculated $DyGa_6C_{63}H_{40}N_9O_{27}$ $[M+H]^{2-}$: 966.84, found 967.85. Elemental analysis of $DyGa_6C_{86}H_{104}N_{13}O_{33}$ [fw = 2428.67 g $mol^{-1}$] calcd (%): C 42.53, H 4.32, N 7.50; found: C 42.48, H 4.21, N 7.60.

*$[HoGa_6(H_2shi)(Hshi)(shi)_7(HNEt_3)_3(C_5H_5N)]\cdot C_5H_5N\cdot 8H_2O$*, **Er-1**: The synthetic yield was 12% based on holmium nitrate pentahydrate. Selected IR peaks (Diamond ATR): $\tilde{\nu}$ = 1654 $cm^{-1}$, 1604 $cm^{-1}$, 1575 $cm^{-1}$, 1525 $cm^{-1}$, 1473 $cm^{-1}$, 1444 $cm^{-1}$, 1391 $cm^{-1}$. 1314 $cm^{-1}$, 1267 $cm^{-1}$, 1154 $cm^{-1}$, 1100 $cm^{-1}$, 1025 $cm^{-1}$, 945 $cm^{-1}$, 920 $cm^{-1}$, 860 $cm^{-1}$, 757 $cm^{-1}$, 672 $cm^{-1}$, 602 $cm^{-1}$. ESI-MS (180 V), calculated $HoGa_6C_{63}H_{40}N_9O_{27}$ $[M+H]^{2-}$: 957.33, found 956.33. ESI-MS (180 V), calculated $HoGa_6C_{63}H_{40}N_9O_{27}$ $[M+H]^{2-}$: 968.34, found 969.35. Elemental analysis of $HoGa_6C_{91}H_{113}N_{14}O_{35}$ [fw = 2546.24 g $mol^{-1}$] calcd (%): C 42.93, H 4.47, N 7.70; found: C 42.63, H 4.38, N 7.64.

*$[ErGa_6(H_2shi)(Hshi)(shi)_7(HNEt_3)_3(C_5H_5N)]\cdot C_5H_5N\cdot 6H_2O$*, **Er-1**: The synthetic yield was 10% based on erbium nitrate pentahydrate. Selected IR peaks (Diamond ATR): $\tilde{\nu}$ = 1654 $cm^{-1}$, 1604 $cm^{-1}$, 1575 $cm^{-1}$, 1525 $cm^{-1}$, 1473 $cm^{-1}$, 1444 $cm^{-1}$, 1391 $cm^{-1}$. 1314 $cm^{-1}$, 1267 $cm^{-1}$, 1154 $cm^{-1}$, 1100 $cm^{-1}$, 1025 $cm^{-1}$, 945 $cm^{-1}$, 920 $cm^{-1}$, 860 $cm^{-1}$, 757 $cm^{-1}$, 672 $cm^{-1}$, 602 $cm^{-1}$. ESI-MS (180 V), calculated $ErGa_6C_{63}H_{40}N_9O_{27}$ $[M+H]^{2-}$: 957.33, found 956.33. ESI-MS (180 V), calculated $ErGa_6C_{63}H_{40}N_9O_{27}$ $[M+H]^{2-}$: 969.34., found 969.85. Elemental analysis of $ErGa_6C_{91}H_{109}N_{14}O_{33}$ [fw = 2512.53 g $mol^{-1}$] calcd (%): C 43.50, H 4.37, N 7.80; found: C 43.39, H 4.36, N 7.78.

*$[TmGa_6(H_2shi)(Hshi)(shi)_7(HNEt_3)_3(C_5H_5N)]\cdot C_5H_5N\cdot 4H_2O$*, **Tm-1**: The synthetic yield was 36% based on thulium nitrate pentahydrate. Selected IR peaks (Diamond ATR): $\tilde{\nu}$ = 1654 $cm^{-1}$, 1604 $cm^{-1}$, 1575 $cm^{-1}$, 1525 $cm^{-1}$, 1473 $cm^{-1}$, 1444 $cm^{-1}$, 1391 $cm^{-1}$. 1314 $cm^{-1}$, 1267 $cm^{-1}$, 1154 $cm^{-1}$, 1100 $cm^{-1}$, 1025 $cm^{-1}$, 945 $cm^{-1}$, 920 $cm^{-1}$, 860 $cm^{-1}$, 757 $cm^{-1}$, 672 $cm^{-1}$, 602 $cm^{-1}$. ESI-MS (180 V), calculated $TmGa_6C_{63}H_{40}N_9O_{27}$ $[M+H]^{2-}$: 957.33, found 956.33. ESI-MS (180 V), calculated $TmGa_6C_{63}H_{40}N_9O_{27}$ $[M+H]^{2-}$: 970.35, found 971.35. Elemental analysis of $TmGa_6C_{91}H_{105}N_{14}O_{31}$ [fw = 2495.64 g $mol^{-1}$] calcd (%): C 44.10, H 4.27, N 7.91; found: C 44.12, H 4.30, N 7.95.

*$[YbGa_6(H_2shi)(Hshi)(shi)_7(HNEt_3)_3(C_5H_5N)]\cdot C_5H_5N\cdot 8H_2O$*, **Yb-1**: The synthetic yield was 24% based on ytterbium nitrate hexahydrate. Selected IR peaks (Diamond ATR): $\tilde{\nu}$ = 1654 $cm^{-1}$, 1604 $cm^{-1}$, 1575 $cm^{-1}$, 1525 $cm^{-1}$, 1473 $cm^{-1}$, 1444 $cm^{-1}$, 1391 $cm^{-1}$. 1314 $cm^{-1}$, 1267 $cm^{-1}$, 1154 $cm^{-1}$, 1100 $cm^{-1}$, 1025 $cm^{-1}$, 945 $cm^{-1}$, 920 $cm^{-1}$, 860 $cm^{-1}$, 757 $cm^{-1}$, 672 $cm^{-1}$, 602 $cm^{-1}$. ESI-MS (180 V), calculated $YbGa_6C_{63}H_{40}N_9O_{27}$ $[M+H]^{2-}$: 957.33, found 956.33. ESI-MS (180 V), calculated $YbGa_6C_{63}H_{40}N_9O_{27}$ $[M+H]^{2-}$: 972.85, found 972.85. Elemental analysis of $YbGa_6C_{91}H_{113}N_{14}O_{35}$ [fw = 2554.36 g $mol^{-1}$] calcd (%): C 42.79, H 4.46, N 7.68; found: C 42.85, H 4.18, N 7.71.

*$LaGa_6(H_2shi)(Hshi)(shi)_7(HNEt_3)_3(C_5H_5N)]\cdot 2C_5H_5N\cdot 4H_2O$*, **La-1**: The synthetic yield was 17% based on lanthinum nitrate pentahydrate. Selected IR peaks (Diamond ATR): $\tilde{\nu}$ = 1654 $cm^{-1}$, 1604 $cm^{-1}$, 1575 $cm^{-1}$, 1525 $cm^{-1}$, 1473 $cm^{-1}$, 1444 $cm^{-1}$, 1391 $cm^{-1}$. 1314 $cm^{-1}$, 1267 $cm^{-1}$, 1154 $cm^{-1}$, 1100 $cm^{-1}$, 1025 $cm^{-1}$, 945 $cm^{-1}$, 920 $cm^{-1}$, 860 $cm^{-1}$, 757 $cm^{-1}$, 672 $cm^{-1}$, 602 $cm^{-1}$. ESI-MS (180 V), calculated $LaGa_6C_{63}H_{40}N_9O_{27}$ $[M+H]^{2-}$: 957.33, found 956.33. ESI-MS (180 V), calculated $LaGa_6C_{63}H_{40}N_9O_{27}$ $[M+H]^{2-}$: 955.33, found 956.33 Elemental analysis of $LaGa_6C_{91}H_{113}N_{14}O_{35}$ [fw = 2527.25 g $mol^{-1}$] calcd (%): C 45.62, H 4.39, N 8.31; found: C 45.75, H 4.33, N 8.34.

*$YGa_6(H_2shi)(Hshi)(shi)_7(HNEt_3)_3(C_5H_5N)]\cdot C_5H_5N\cdot 2H_2O$*, **Y-1**: The synthetic yield was 44% based on yttrium nitrate hexahydrate. Selected IR peaks (Diamond ATR): $\tilde{\nu}$ = 1654 $cm^{-1}$, 1604 $cm^{-1}$, 1575 $cm^{-1}$, 1525 $cm^{-1}$, 1473 $cm^{-1}$, 1444 $cm^{-1}$, 1391 $cm^{-1}$. 1314 $cm^{-1}$, 1267 $cm^{-1}$, 1154 $cm^{-1}$, 1100 $cm^{-1}$, 1025 $cm^{-1}$, 945 $cm^{-1}$, 920 $cm^{-1}$, 860 $cm^{-1}$, 757 $cm^{-1}$, 672 $cm^{-1}$, 602 $cm^{-1}$. ESI-MS (180 V), calculated $YGa_6C_{63}H_{40}N_9O_{27}$ $[M+H]^{2-}$: 957.33, found 956.33. ESI-MS (180 V), calculated $YGa_6C_{63}H_{40}N_9O_{27}$ $[M+H]^{2-}$: 930.33, found 931.32. Elemental analysis of $YGa_6C_{91}H_{101}N_{14}O_{29}$ [fw = 2362.12 g $mol^{-1}$] calcd (%): C 46.27, H 4.31, N 8.30; found: C 46.25, H, 4.56, N 8.32.

*$LuGa_6(H_2shi)(Hshi)(shi)_7(HNEt_3)_3(C_5H_5N)]\cdot C_5H_5N\cdot 3H_2O$*, **Lu-1**: The synthetic yield was 39% based on lutetium nitrate hydrate. Selected IR peaks (Diamond ATR): $\tilde{\nu}$ = 1654 $cm^{-1}$, 1604 $cm^{-1}$, 1575 $cm^{-1}$, 1525 $cm^{-1}$, 1473 $cm^{-1}$, 1444 $cm^{-1}$, 1391 $cm^{-1}$. 1314 $cm^{-1}$, 1267 $cm^{-1}$, 1154 $cm^{-1}$, 1100 $cm^{-1}$, 1025 $cm^{-1}$, 945 $cm^{-1}$, 920 $cm^{-1}$, 860 $cm^{-1}$, 757 $cm^{-1}$, 672 $cm^{-1}$, 602 $cm^{-1}$. ESI-MS (180 V), calculated $LuGa_6C_{63}H_{40}N_9O_{27}$ $[M+H]^{2-}$: 957.33, found 956.33. ESI-MS (180 V), calculated $LuGa_6C_{63}H_{40}N_9O_{27}$ $[M+H]^{2-}$: 973.35, found 974.36. Elemental analysis of $LuGa_6C_{91}H_{103}N_{14}O_{30}$ [fw = 2466.20 g $mol^{-1}$] calcd (%): C 44.32, H 4.21, N 7.98; found: C 44.27, H 4.30, N 7.95.

**Physical methods**: ESI-QTOF MS was performed on an Agilent 6520 Accurate-Mass Q-TOF LC/MS quadrupole time of flight mass spectrometer in negative ion mode with a fragmentation voltage of 180 V. Samples were prepared by dissolving approximately 1 mg of compound in 1 mL of methanol, then diluting 20 μL of this first solution into another 1 mL of methanol. Samples were directly injected using a syringe (without the HPLC or autosampler). Data were processed with the Agilent MassHunter Qualitative Analysis software. Elemental analyses were performed on a Carlo Erba 1108 or a PerkinElmer 2400 elemental analyzer by Atlantic Microlabs, Inc.

**$^1$H NMR spectroscopy**: $^1$H NMR spectra were collectued using a 400 MHz Varian MR400 spectrometer at room temperature. Samples were dissolved in [$D_5$]pyridine and collected using a standard proton pulse sequence, Spectra were processed using MestraNova 6.0 software.

**FT-IR spectroscopy**: Solid state FT-IR spectra were collected using a Thermo Scientific Nicolet iS50 FT-IR spectrometer with a Pike MIRacle diamond ATR accessory. Spectra were collected using X scans and subtracting a background spectra collected at ambient conditions.

**Powder X-ray diffraction**: Samples were ground using a mortar and pestle and then loaded onto glass plates such that the surface of the sample was as flat as possible. Data were collected using a PANalytical Emyprean Series 2 XRD with a 1.54243 Å Cu anode source and an operational tension of 45 kV and current of 40 mA. The collection range was 3 to 15° in 2θ with step size of 0.016711° and a scan speed of 0.2 seconds per step.

**X-ray crystallography**: Single crystal X-ray crystallographic data for **Tb-1** were collected at 85(2) K on an AFC10K Saturn 944+ CCD-based X-ray diffractometer equipped with a Micromax007HF Cu-target microfocus rotating anode ($\lambda$ = 1.54187 Å), operated at 1200 W (40 kV, 30 mA). The data were processed using CrystalClear 2.0[70] and corrected for absorption. The structure was solved and refined using the SHELXTL (v. 6.12) software package.[71] Non-hydrogen atoms were refined anisotropically, hydrogen atoms were isotropic and placed in idealized positions.

**Photophysical measurements**: Luminescence data were collected on samples in the solid state placed in 2.4 mm i.d. quartz capillaries. Emission and excitation spectra were measured on a custom-designed Horiba Scientific Fluorolog 3 spectrofluorimeter equipped with either a visible photomultiplier tube (PMT) (220–850 nm, R928P; Hamamatsu), a NIR solid-state InGaAs detector cooled to 77 K (800–1600 nm, DSS-IGA020L; Horiba Scientific), or a NIR PMT (950–1650 nm, H10330-75; Hamamatsu). Excitation and emission spectra were corrected for the instrumental functions. Luminescence lifetimes were determined under excitation at 355 nm provided by a Nd:YAG laser (YG 980; Quantel). Signals were detected in the visible or NIR ranges with the help of a Hamamatsu R928P or H10330-75 PMTs, respectively. The output signals obtained from

the detectors were fed into a 500 MHz bandpass digital oscilloscope (TDS 754C; Tektronix), transferred to a PC for data processing with the program Origin 8. Luminescence lifetimes are averages of at least three independent measurements. Quantum yields were determined with a Fluorolog 3 spectrofluorimeter based on an absolute method with the help of an integration sphere (Model G8, GMP SA, Renens, Switzerland). Each sample was measured several times under comparable experimental conditions, varying the position of the sample. Estimated experimental error for quantum yield determination is ~10%.

**Absorption spectroscopy**: Solution-state UV-vis spectra were collected on samples dissolved in methanol (approx. 300 μM) using a Cary 100Bio UV/Vis spectrophotometer in absorbance mode. Solid-state spectra were recorded using an Agilent-Cary 5000 spectrophotometer equipped with a Praying Mantis diffuse reflectance attachment in reflectance mode. Samples were milled in $BaSO_4$ (1:9 sample:$BaSO_4$ w/w), and a baseline of 100% $BaSO_4$ was used for correction. Reflectance was converted to absorption using the Kubelka-Munk function.

**Magnetic characterization**: AC-magnetic susceptibility was collected using a Quantum Design MPMS SQUID magnetometer. Samples were prepared in gel capsules and suspended in eicosane (1:2 sample:eicosane w/w). DC magnetic susceptibility was corrected for the capsule, eicosane and sample holder, as well as for diamagnetic contributions using Pascal's constants. Data were processed using Microsoft Excel and SigmaPlot 10 software packages. The temperature and frequency dependent AC out of phase susceptibility, Arrhenius plot and Cole–Cole plot were fit using least squares methods with SigmaPlot 10.

## *Acknowledgements*

This work was supported by the National Science Foundation under grant CHE-1361799 to V.L.P. and J.C.L.. The authors would also like to acknowledge the funding from the European Community's Seventh Framework Program (FP7/2007–2013) (no. 611488), la Ligue Contre le Cancer, la Région Centre, le Cancéropôle Grand Ouest and l'Agence Nationale de la Recherche (ANR-12-BS07-0012 and ANR-13-BS08-0011). S.P. acknowledges support from the Institut National de la Santé et de la Recherche Médicale (INSERM).

## Conflict of interest

The authors declare no conflict of interest.

**Keywords:** cryptands · lanthanides · luminescence · magnetic properties · spectroscopy

[1] J.-C. G. Bünzli, S. V. Eliseeva in *Springer Series on Fluorescence. Lanthanide Luminescence: Photophysical, Analytical and Biological Aspects* (Eds.: P. Hanninen, H. Harma), Springer, Berlin, **2011**, pp. 1–45.
[2] S. V. Eliseeva, J.-C. G. Bünzli, *Chem. Soc. Rev.* **2010**, *39*, 189–227.
[3] J. -C. G. Bünzli, S. V. Eliseeva, *J. Rare Earths* **2010**, *28*, 824–842.
[4] A. J. Amoroso, S. J. A. Pope, *Chem. Soc. Rev.* **2015**, *44*, 4723–4742.
[5] I. Martinić, S. V. Eliseeva, S. Petoud, *J. Lumin.* **2017**, *189*, 19–43.
[6] K. Binnemans, *Chem. Rev.* **2009**, *109*, 4283–4374.
[7] S. V. Eliseeva, J.-C. G. Bünzli, *New J. Chem.* **2011**, *35*, 1165–1176.
[8] M. Sy, A. Nonat, N. Hildebrandt, L. J. Charbonnière, *Chem. Commun. (Camb).* **2016**, *52*, 5080–5095.
[9] E. R. Trivedi, S. V. Eliseeva, J. Jankolovits, M. M. Olmstead, S. Petoud, V. L. Pecoraro, *J. Am. Chem. Soc.* **2014**, *136*, 1526–1534.
[10] H. Uh, S. S. S. Petoud, H. Uha, S. S. S. Petoud, H. Uh, S. S. S. Petoud, *Comptes Rendus Chim.* **2010**, *13*, 668–680.
[11] S. Comby, J.-C. G. Bünzli in *Handb. Phys. Chem. Rare Earths, Vol 37 Opt. Spectrosc.* (Eds.: K. A. Gschneidner, J.-C. G. Bünzli, V. K. Pecharsky), Elsevier Science Amsterdam, **2007**.
[12] S. Petoud, G. Muller, E. G. Moore, J. Xu, J. Sokolnicki, J. P. Riehl, U. N. Le, S. M. Cohen, K. N. Raymond, *J. Am. Chem. Soc.* **2007**, *129*, 77–83.
[13] J. Zhang, P. D. Badger, S. J. Geib, S. Petoud, *Angew. Chem. Int. Ed.* **2005**, *44*, 2508–2512; *Angew. Chem.* **2005**, *117*, 2564–2568.
[14] C. Y. Chow, S. V. Eliseeva, E. R. Trivedi, T. N. Nguyen, J. W. Kampf, S. Petoud, V. L. Pecoraro, *J. Am. Chem. Soc.* **2016**, *138*, 5100–5109.
[15] S. Biju, Y. K. Eom, J.-C. G. Bünzli, H. K. Kim, *J. Mater. Chem. C* **2013**, *1*, 3454–3466.
[16] G. L. Law, T. A. Pham, J. Xu, K. N. Raymond, *Angew. Chem. Int. Ed.* **2012**, *51*, 2371–2374; *Angew. Chem.* **2012**, *124*, 2421–2424.
[17] N. Wartenberg, O. Raccurt, E. Bourgeat-Lami, D. Imbert, M. Mazzanti, *Chem. Eur. J.* **2013**, *19*, 3477–3482.
[18] S. Quici, M. Cavazzini, G. Marzanni, G. Accorsi, N. Armaroli, B. Ventura, F. Barigelletti, *Inorg. Chem.* **2005**, *44*, 529–537.
[19] T. N. Nguyen, C. Y. Chow, S. V. Eliseeva, E. R. Trivedi, J. W. Kampf, I. Martinić, S. Petoud, V. L. Pecoraro, *Chem. Eur. J.* **2018**, *24*, 1031–1035.
[20] R. E. P. Winpenny, *Angew. Chem. Int. Ed.* **2008**, *47*, 7992–7994; *Angew. Chem.* **2008**, *120*, 8112–8114.
[21] L. Bogani, W. Wernsdorfer, *Nat. Mater.* **2008**, *7*, 179–186.
[22] C. Benelli, D. Gatteschi, *Chem. Rev.* **2002**, *102*, 2369–2388.
[23] L. Sorace, C. Benelli, D. Gatteschi, *Chem. Soc. Rev.* **2011**, *40*, 3092.
[24] N. Ishikawa, M. Sugita, T. Ishikawa, S. Koshihara, Y. Kaizu, *J. Am. Chem. Soc.* **2003**, *125*, 8694–8695.
[25] M. A. AlDamen, S. Cardona-Serra, J. M. Clemente-Juan, E. Coronado, A. Gaita-Ariño, C. Martí-Gastaldo, F. Luis, O. Montero, *Inorg. Chem.* **2009**, *48*, 3467–3479.
[26] J. D. Rinehart, J. R. Long, *Chem. Sci.* **2011**, *2*, 2078.
[27] V. L. Pecoraro, *Inorg. Chim. Acta* **1989**, *155*, 171–173.
[28] M. S. Lah, V. L. Pecoraro, *J. Am. Chem. Soc.* **1989**, *111*, 7258–7259.
[29] J. T. Grant, J. Jankolovits, V. L. Pecoraro, *Inorg. Chem.* **2012**, *51*, 8034–8041.
[30] J. Jankolovits, A. D. Cutland Van-Noord, J. W. Kampf, V. L. Pecoraro, *Dalton Trans.* **2013**, *42*, 9803.
[31] C.-S. Lim, M. Tegoni, T. Jakusch, J. W. Kampf, V. L. Pecoraro, *Inorg. Chem.* **2012**, *51*, 11533–11540.
[32] C. Atzeri, L. Marchiò, C. Y. Chow, J. W. Kampf, V. L. Pecoraro, M. Tegoni, *Chem. Eur. J.* **2016**, *22*, 6482–6486.
[33] C. M. Zaleski, E. C. Depperman, J. W. Kampf, M. L. Kirk, V. L. Pecoraro, *Inorg. Chem.* **2006**, *45*, 10022–10024.
[34] C. M. Zaleski, S. Tricard, E. C. Depperman, W. Wernsdorfer, T. Mallah, M. L. Kirk, V. L. Pecoraro, *Inorg. Chem.* **2011**, *50*, 11348–11352.
[35] C. M. Zaleski, J. W. Kampf, T. Mallah, M. L. Kirk, V. L. Pecoraro, *Inorg. Chem.* **2007**, *46*, 1954–1956.
[36] T. T. Boron, J. W. Kampf, V. L. Pecoraro, *Inorg. Chem.* **2010**, *49*, 9104–9106.
[37] C. Y. Chow, H. Bolvin, V. E. Campbell, R. Guillot, J. W. Kampf, W. Wernsdorfer, F. Gendron, J. Autschbach, V. L. Pecoraro, T. Mallah, *Chem. Sci.* **2015**, *6*, 4148–4159.
[38] Q.-W. Li, J.-L. Liu, J.-H. Jia, Y.-C. Chen, J. Liu, L.-F. Wang, M.-L. Tong, *Chem. Commun.* **2015**, *51*, 10291–10294.
[39] J. Jankolovits, C. M. Andolina, J. W. Kampf, K. N. Raymond, V. L. Pecoraro, *Angew. Chem. Int. Ed.* **2011**, *50*, 9660–9664; *Angew. Chem.* **2011**, *123*, 9834–9838.
[40] G. Mezei, C. M. Zaleski, V. L. Pecoraro, *Chem. Rev.* **2007**, *107*, 4933–5003.
[41] C. M. Zaleski, C.-S. Lim, A. D. Cutland-Van Noord, J. W. Kampf, V. L. Pecoraro, *Inorg. Chem.* **2011**, *50*, 7707–7717.
[42] M. R. Azar, T. T. Boron, J. C. Lutter, C. I. Daly, K. A. Zegalia, R. Nimthong, G. M. Ferrence, M. Zeller, J. W. Kampf, V. L. Pecoraro, C. M. Zaleski, *Inorg. Chem.* **2014**, *53*, 1729–1742.
[43] B. R. Gibney, A. J. Stemmler, S. Pilotek, J. W. Kampf, V. L. Pecoraro, *Inorg. Chem.* **1993**, *32*, 6008–6015.
[44] C. Y. Chow, E. R. Trivedi, V. Pecoraro, C. M. Zaleski, *Comments Inorg. Chem.* **2015**, *35*, 214–253.

[45] M. S. Lah, B. R. Gibney, D. L. Tierney, J. E. Penner-Hahn, V. L. Pecoraro, *J. Am. Chem. Soc.* **1993**, *115*, 5857 – 5858.
[46] C. Dendrinou-Samara, M. Alexiou, C. M. Zaleski, J. W. Kampf, M. L. Kirk, D. P. Kessissoglou, V. L. Pecoraro, *Angew. Chem. Int. Ed.* **2003**, *42*, 3763 – 3766; *Angew. Chem.* **2003**, *115*, 3893 – 3896.
[47] D. P. Kessisoglou, J. Kampf, V. L. Pecoraro, *Polyhedron* **1994**, *13*, 1379 – 1391.
[48] T. Afrati, C. Dendrinou-Samara, C. M. Zaleski, J. W. Kampf, V. L. Pecoraro, D. P. Kessissoglou, *Inorg. Chem. Commun.* **2005**, *8*, 1173 – 1176.
[49] L. Jin, H. Yu, S. Wu, F. Xiao, *Dalton Trans.* **2009**, 197 – 201.
[50] A. W. Addison, T. N. Rao, J. Reedijk, J. van Rijn, G. C. Verschoor, *J. Chem. Soc. Dalton Trans.* **1984**, 1349 – 1356.
[51] R. W. Saalfrank, H. Maid, A. Scheurer, *Angew. Chem. Int. Ed.* **2008**, *47*, 8794 – 8824; *Angew. Chem.* **2008**, *120*, 8924 – 8956.
[52] Ref. [28].
[53] C. M. Zaleski, E. C. Depperman, C. Dendrinou-Samara, M. Alexiou, J. W. Kampf, D. P. Kessissoglou, M. L. Kirk, V. L. Pecoraro, *J. Am. Chem. Soc.* **2005**, *127*, 12862 – 12872.
[54] V. L. Pecoraro, S. V. Eliseeva, S. Petoud, I. Martinic, T. Nguyen, *Simultaneous Cell Fixing and Staining with Metallacrown Complexes.*, n.d., EFS ID 62205053.
[55] I. Martinić, S. V. Eliseeva, T. N. Nguyen, V. L. Pecoraro, S. Petoud, *J. Am. Chem. Soc.* **2017**, *139*, 8388 – 8391.
[56] I. Martinić, S. V. Eliseeva, T. N. Nguyen, F. Foucher, D. Gosset, F. Westall, V. L. Pecoraro, S. Petoud, *Chem. Sci.* **2017**, *8*, 6042 – 6050.
[57] W. T. Carnall, P. R. Fields, K. Rajnak, *J. Chem. Phys.* **1968**, *49*, 4447 – 4449.
[58] W. T. Carnall, P. R. Fields, K. Rajnak, *J. Chem. Phys.* **1968**, *49*, 4424 – 4442.
[59] M. L. Kahn, R. Ballou, P. Porcher, O. Kahn, J. Sutter, *Chem. Eur. J.* **2002**, *8*, 525 – 531.
[60] G. Abbas, Y. Lan, G. E. Kostakis, W. Wernsdorfer, C. E. Anson, A. K. Powell, *Inorg. Chem.* **2010**, *49*, 8067 – 8072.
[61] F. Gao, L. Cui, Y. Song, Y.-Z. Li, J.-L. Zuo, *Inorg. Chem.* **2014**, *53*, 562 – 567.
[62] S. Osa, T. Kido, N. Matsumoto, N. Re, A. Pochaba, J. Mrozinski, *J. Am. Chem. Soc.* **2004**, *126*, 420 – 421.
[63] J. Tang, I. Hewitt, N. T. Madhu, G. Chastanet, W. Wernsdorfer, C. E. Anson, C. Benelli, R. Sessoli, A. K. Powell, *Angew. Chem. Int. Ed.* **2006**, *45*, 1729 – 1733; *Angew. Chem.* **2006**, *118*, 1761 – 1765.
[64] R. Bagai, G. Christou, *Chem. Soc. Rev.* **2009**, *38*, 1011 – 1026.
[65] N. Ishikawa, M. Sugita, W. Wernsdorfer, *Angew. Chem. Int. Ed.* **2005**, *44*, 2931 – 2935; *Angew. Chem.* **2005**, *117*, 2991 – 2995.
[66] A. Lannes, D. Luneau, *Inorg. Chem.* **2015**, *54*, 6736 – 6743.
[67] S. Demir, I.-R. Jeon, J. R. Long, T. D. Harris, *Coord. Chem. Rev.* **2014**, 1 – 28.
[68] J. J. Baldoví, Y. Duan, R. Morales, A. Gaita-Ariño, E. Ruiz, E. Coronado, *Chem. Eur. J.* **2016**, *22*, 13532 – 13539.
[69] J. J. Baldoví, J. M. Clemente-Juan, E. Coronado, A. Gaita-Ariño, *Polyhedron* **2013**, *66*, 39 – 42.
[70] CrystalClear Expert 2.0 r16, Rigaku Americas and Rigaku Corporation (2014), Rigaku Americas, 9009, TX, USA 77381 – 75209, Rigaku Tokyo, 196 – 8666, Japan.
[71] G. M. Sheldrick, *Acta Crystallogr. Sect. A* **2008**, *64*, 112 – 122.

Manuscript received: March 16, 2018
Accepted manuscript online: May 16, 2018
Version of record online: June 27, 2018